Heliyon 10 (2024) e33675

Contents lists available at ScienceDirect

Heliyon

journal homepage: www.cell.com/heliyon

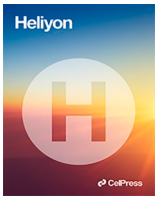

Research article

Acupuncture improve proteinuria in diabetic kidney disease rats by inhibiting ferroptosis and epithelial-mesenchymal transition

J.I. Yue [a,b,1], Z.H.A.N.G. Xin-yuan [a,1], X.I.A.O. Yun-ming [c,d,1], Z.H.U.A.N.G. Zi-hao [a], Y.A.N.G. Xiao-hui [a], L.I. Xin-ju [a,*]

[a] College of Traditional Chinese Medicine, Tianjin University of Traditional Chinese Medicine, Tianjin, 301617, PR China
[b] Dongzhimen Hospital, Beijing University of Traditional Chinese Medicine, Institute of Nephrology & Beijing Key Laboratory, Beijing, 100700, PR China
[c] Department of Nephrology, Medical School of Chinese PLA, First Medical Center of Chinese PLA General Hospital, Nephrology Institute of the Chinese People's Liberation Army, State Key Laboratory of Kidney Diseases, National Clinical Research Center for Kidney Diseases, Beijing, PR China
[d] Key Laboratory of Kidney Disease Research, Beijing, 100000, PR China

ARTICLE INFO

Keywords:
Acupuncture
Diabetic kidney disease
Ferroptosis

ABSTRACT

Objective: To explore the mechanism of acupuncture to relieve diabetic proteinuria in Diabetic Kidney Disease (DKD).

Methods: A total of 10 male Sprague-Dawley rats were randomly selected as the negative control group (NC), and a further 30 rats were fed a high-fat diet (HFD) and intraperitoneal streptozotocin (STZ). The DKD model rats in the model group (DKD) and the acupuncture group (DKD + Acu) were randomly assigned. After 4 weeks of intervention, collected urine, peripheral blood, and renal tissues from all rats, and assessed blood urea nitrogen, serum creatinine, triglyceride, 24-h urine protein quantification, and blood glucose, left kidney weight, kidney body ratio index, then observe changes in renal histology in the rats. The renal cortex tissues of three rats from each group were sent for transcriptomic analysis. According to the results of transcriptomic analysis, various kits were used to detect SOD, MDA, GSH, GSH-px, and iron concentration. The expression levels of GPX4 and System Xc-, members of the antioxidative stress pathway, and TfR 1, SLC39A14, FTH 1, and SLC40A1, involved in iron metabolism, in the kidney tissues were measured by western blotting and reverse transcription-quantitative PCR. The expression of mesenchymal phenotype markers and podocyte-specific markers were evaluated by immunofluorescence.

Results: Acupuncture promoted the levels of GSH, GSH-px, and SOD, decreased the level of MDA ($P < 0.05$), promoted the expression of GPX4 and System Xc- ($P < 0.05$), decreased the expression of TfR1 and SLC39A14 ($P < 0.01$), and increased the expression of FTH 1 and SLC40A1 ($P < 0.05$), inhibited the expression of TGF-β1, desmin, FSP-1, and α-SMA ($P < 0.05$), promoted the expression of Nephrin, Podocin, and CD2AP ($P < 0.05$).

Conclusion: Improving the ability of podocytes to prevent oxidative stress and restoring iron ion homeostasis, can improve Ferroptosis and block epithelial-mesenchymal transition, improve podocyte injury, restore filtration function, and reduce proteinuria in DKD rats.

* Corresponding author.
E-mail address: lixinju@tjutcm.edu.cn (L.I. Xin-ju).
[1] These authors contribute equally to the article.

https://doi.org/10.1016/j.heliyon.2024.e33675
Received 25 March 2024; Received in revised form 24 June 2024; Accepted 25 June 2024
Available online 2 July 2024

1. Introduction

Diabetic Kidney Disease (DKD) refers to renal microvascular complications induced by diabetes, leading to clinical manifestations primarily characterized by proteinuria and progressive decline in renal function. DKD is the major reason for renal function impairment and End-Stage Renal Disease (ESRD) in diabetic patients [1]. The International Diabetes Federation (IDF) states that in 2021, the global prevalence of diabetes among adults was 10.5 %, translating to 536.6 million people. Furthermore, the IDF predicts this figure will increase to 12.2 % (783.2 million people) by 2045 [2]. With the increasing prevalence of diabetes worldwide, DKD has become one of the most challenging health issues. Despite implementing various treatment approaches such as glycemic control, blood pressure management, the use of renin-angiotensin-aldosterone system (RAAS) inhibitors, and sodium-glucose co-transporter 2 (SGLT-2) inhibitors in clinical practice, the overall effectiveness remains insufficient for various reasons [3]. Therefore, ongoing exploration of treatment modalities remains of significant importance.

The primary mechanism underlying DKD is the loss of podocyte foot processes, leading to damage to the glomerular filtration barrier and the production of albuminuria. High glucose levels can trigger the growth of mesangial cells and collagen synthesis in the matrix, which can result in the development of pathological characteristics of DKD, including podocyte loss, thickening of the basement membrane, accumulation of interstitial matrix, and fibrosis of the renal interstitium [4]. It has been found that the pathogenesis of DKD is linked to the activation of multiple signaling pathways, and recent evidence suggests that ferroptosis is closely associated with DKD [5].

Ferroptosis is a mode of cellular death that differs from apoptosis and is characterized by an iron-dependent environment marked by oxidative imbalances, compromised antioxidant functionality, and increased lipid peroxidation byproducts. Morphologically, it is characterized by cell membrane rupture or blebbing, mitochondrial shrinkage, increased membrane density, and decreased or the

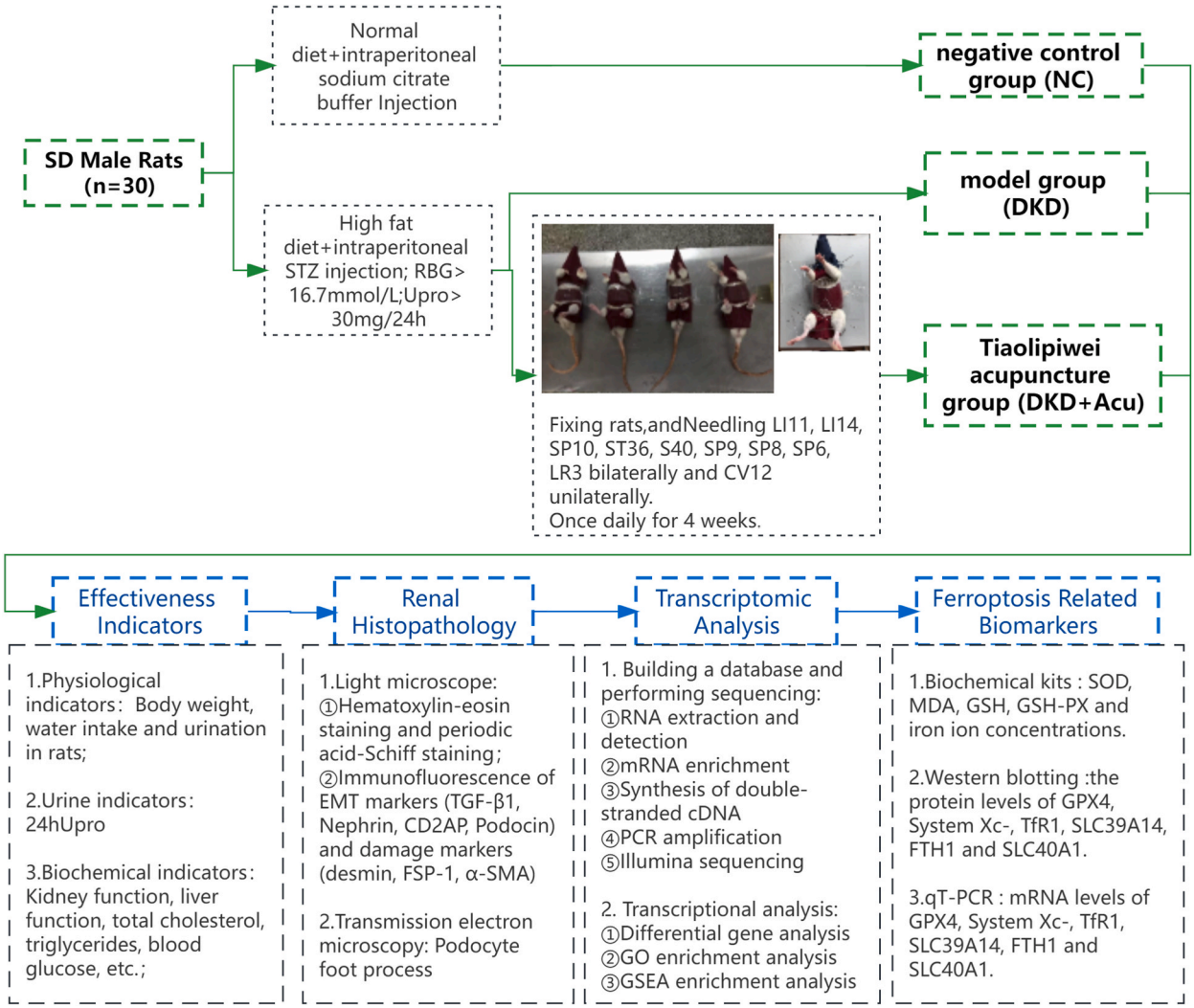

Fig. 1. Flowchart of the experimental setup in the present study.

disappearance of mitochondrial cristae [6]. The build-up of lipid peroxidation byproducts is generally considered a consequential aspect of ferroptosis, which can cause the breakdown of cellular membrane integrity. Upstream processes of lipid metabolism, iron metabolism, and oxidative stress are closely related to the downstream results of lipid peroxidation [7].

Traditional Chinese medicine (TCM), with its extensive history, has played a crucial role in advancing medical care. In the treatment of DKD, TCMs have demonstrated commendable clinical efficacy [8]. Acupuncture, an integral component of TCM, has the potential to enhance renal function, minimize proteinuria, regulate hypertension, and deliver therapeutic benefits for various forms of kidney diseases [9].

The efficacy of acupuncture is closely related to the selection and compatibility of acupoints. Zhang et al. [10], responsible for the well-established Tianjin TCM and National Well-known Veteran TCM Experts Inheritance Studio, has established the "Tiao li pi wei" (TLPW) acupuncture method to treat DKD through long-term clinical practice. Previous clinical studies have shown that the TLPW acupuncture method can improve 24-h urinary protein in patients with early DKD. Basic experimental studies have shown that this therapy can improve a patient's ability to resist oxidative stress and delay the progression of DKD [11]. Additionally, by establishing a DKD rat model, the team found that this therapy can improve podocyte structure, enhance kidney function, and reduce urinary protein in rats [12].

The experimental workflow used in the present study (shown in Fig. 1). First, type 2 DKD was induced in rats. The rats were subsequently divided into treatment and control groups for further investigation. After 4 weeks of TLPW acupuncture intervention in the treatment group, samples were subjected to sequencing. Transcriptomic analysis revealed that several potential pathways, including iron ion binding, antioxidant stress, epithelial-mesenchymal transition (EMT), and actin-binding, were significantly associated with the treatment, confirming their close relationship with ferroptosis. Subsequently, validation was conducted through animal experiments and molecular biology-based methods.

It was found that TLPW acupuncture mitigated podocyte EMT, and inhibited podocyte ferroptosis through the GPX4/System Xc- antioxidant stress pathway and the TfR1/SLC39A14/FTH1/SLC40A1 iron ion transport pathway, improved podocyte damage, enhanced kidney function, and reduced proteinuria in DKD rats, providing evidence for the effectiveness of the treatment.

2. Materials and methods

Ethical statement

The procedures recommended in the Guide for the Care and Use of Laboratory Animals (National Institutes of Health, 8th edition, 2011 update) were diligently followed throughout the course of this study. The study protocol was approved by the Ethics Committee of the Institute of Radiation Medicine, Chinese Academy of Medical Sciences (approval no. IRM-DWLL-2019103).

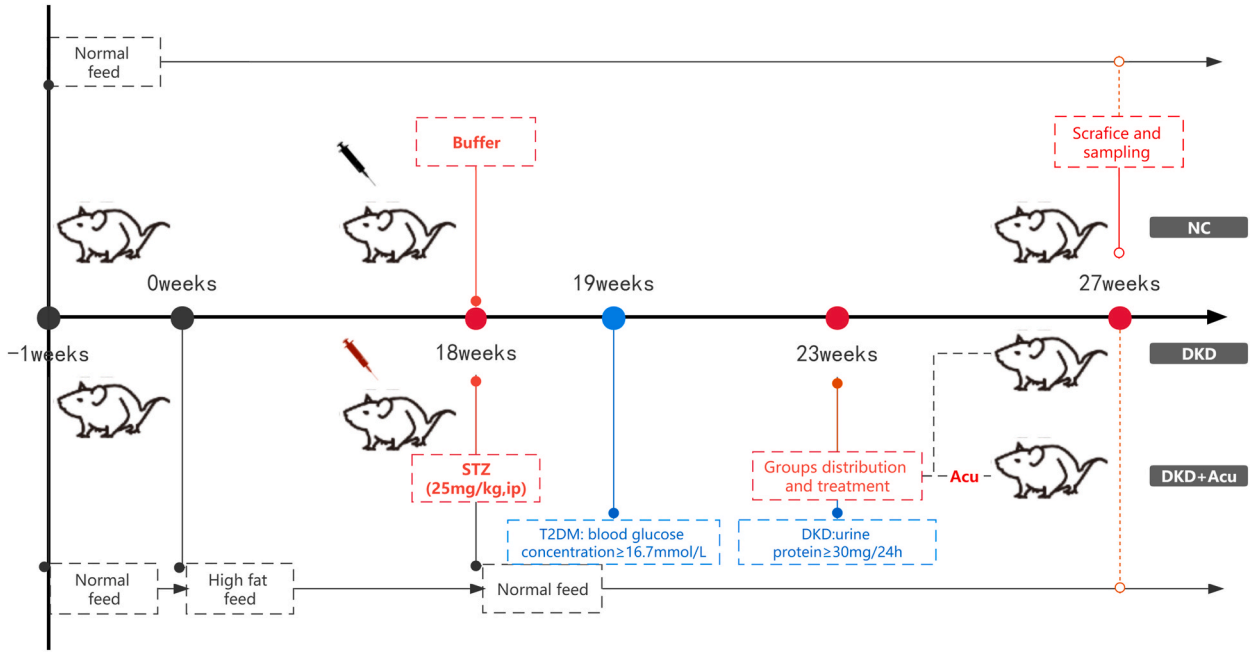

Fig. 2. Operational flowchart for the establishment of the animal model.

2.1. Animals

A total of 30 male Sprague-Dawley (SD) rats [HuaFukang Laboratory Animal Company, SCXK (Beijing) 2019-0009] weighing between 170 and 210 g were individually housed in a windowless and temperature-controlled room at 23 ± 2 °C with a humidity level of 55 ± 10 %. The rats were provided *ad libitum* access to water and food and subjected to a 12h light/dark cycle (lights on at 7 a.m. to simulate daylight conditions).

2.2. Grouping and intervention

A total of 10 healthy male SD rats were randomly selected as the negative control (NC) group and fed a regular diet. The remaining 20 rats were fed a high-fat diet (HFD). Following 18 weeks of feeding, the group of rats designated as the control received a sole intraperitoneal injection of 25 mg/kg citrate buffer (n = 10) (Beijing Solarbio Science & Technology Co., Ltd.). The remaining 10 rats that were fed an HFD were administered 25 mg/kg streptozotocin (STZ, dissolved in 0.1 M citrate buffer, pH4.3) (Millipore Sigma) and subsequently fed with a regular diet [13]. A total of 1 week after the injection, rats in the HFD group who consistently displayed tail blood glucose levels ≥16.7 mmol/l for 3 consecutive days were diagnosed with type 2 diabetes. At week 5 after injection, metabolic cages were used to collect urine from the rats, and 24-h urine protein quantification was measured. Rats with 24-h urinary protein levels ≥30 mg were considered indicative of the successful establishment of a model of DKD (shown in Fig. 2).

2.3. Procedure of TLPW acupuncture

The rats were placed in the supine and immobilized with a non-obstructive restraint so as not to affect respiration. Then, they were fixed to the operating table with adhesive tape. The specific location and needle insertion method for TLPW acupuncture were as follows: LI1, insert the needle vertically ~3 mm in the depression on the lateral anterior aspect of the proximal end of the radius; LI4, insert the needle vertically ~1 mm in the depression between the first and second metacarpal bones of the forelimb; SP10, insert the needle vertically ~2 mm at the lower 1/9 point of the line connecting the inner corner of the knee and the pubic symphysis on the inner side of the hind leg; ST36, insert the needle vertically ~3 mm below the head of the fibula on the outer side of the knee joint; S40, insert the needle vertically ~4 mm in the middle of the calf bone on the posterior edge of the fibula; SP9, insert the needle vertically ~2 mm in the depression below the posterior medial condyle of the tibia in the lower leg; SP8, insert the needle vertically ~3 mm directly below the medial condyle of the tibia in the lower leg; SP6, insert the needle vertically ~3 mm above the medial malleolus of the hind leg; LR3, insert the needle vertically ~1 mm in the depression between the first and second metatarsal bones on the dorsal surface of the hind paw; and CV12, insert the needle vertically ~4 mm above the navel. Except for CV12, all acupoints were needled bilaterally. After routine disinfection of the acupoints, the needles were inserted perpendicularly without manipulation and left for 30 min. The rats received one acupuncture treatment per day for 4 consecutive weeks.

2.4. Grouping method

Following successful modeling, rats that met the DKD modeling criteria were randomly allocated to one of two groups, a DKD group and a DKD + Acu group. The DKD group did not receive any other intervention, while the DKD + Acu group received daily TLPW needling acupuncture intervention for 30 min per session. Over 4 weeks, the random blood glucose and weight of the rats were measured and recorded weekly. After 4 weeks, all rats were anesthetized with 30 mg/kg pentobarbital (Huanaite Biotechnology Co., Ltd.) and euthanized by cervical dislocation to collect blood samples and kidney tissues for further analysis.

2.4.1. Analysis of urine and blood-related indicators

Tail blood was collected before modeling and weekly after intervention for biochemical tests using a blood glucose meter (Accu-Chek; Roche Diagnostics) to detect rat blood glucose levels. 24 h urine samples were gathered using metabolic cages to evaluate 24-h urinary protein levels with a urine protein quantification test kit (Beijing Solarbio Technology Co., Ltd.).

All experimental rats were anesthetized to collect abdominal aortic blood samples in the fourth week following the intervention. The collected blood samples were then centrifuged at 1509.3×*g* for 15 min, and the resulting serum was carefully extracted and stored at a temperature of −80 °C for further analysis. Multiple biochemical test kits (Nanjing Jiancheng Biological Engineering Research Institute Co., Ltd.) were used to measure blood urea nitrogen (cat.no.C013-2-1), serum creatinine (cat.no.C011-2-1), triglycerides (cat. no.A110-1-1), total cholesterol (cat.no.C111-1-1), total protein(cat.no.A045-2-2), and albumin levels(cat.no.A028-2-1). Anthropometric measurements such as body weight, kidney weight, and kidney weight/body weight ratio were taken into account. The left kidney index (LKW/BW) was calculated as the left kidney weight/body weight x 100 %.

2.5. Histopathology and immunofluorescence analysis

Renal tissues from anesthetized rats were fixed, embedded, dewaxed and cut into slices of ~5 μM. Hematoxylin-eosin staining (HE, Beijing BIOSS Biotechnology Co., Ltd.), periodic acid-Schiff staining (PAS, Microscopy PAS Staining Kit, MilliporeSigma) and prussian blue iron staining (Prussian Blue Iron Stain Kit, Enhance With DAB, Beijing Solarbio Technology Co., Ltd.) were then performed, and the kidney tissue was observed under an optical microscope to assess the pathological changes.

Some other renal tissues were fixed, dehydrated, embedded, and sliced for electron microscopy analysis. Using a transmission

electron microscope (Olympus Corporation), the degree of podocyte injury was assessed by observing the number, width, and thickness of the foot processes and the glomerular basement membrane. Additionally, using the same transmission electron microscope, the size, shape, and integrity of the mitochondria were documented.

For immunofluorescence, the paraffin sections were dewaxed and rehydrated, after which antigen retrieval was performed. The primary and secondary antibodies were added in sequence. Images were obtained under a microscope, and ImageJ software (National Institutes of Health) was used for semi-quantitative fluorescence analysis in the glomerular area. A total of three randomly selected fluorescence sections of the kidney from each group of rats were measured to detect the expression of TGF-β1 (cat.no. bs-0086R,1:100), Desmin (cat.no. bs-20702R,1:100), α-SMA (cat.no. bs-10196R,1:100), Fsp1 (cat.no. bs-3759R,1:100), nephrin (cat.no. bs-4866R,1:100), podocin (cat.no. bs-6597R1:100), and CD2AP (cat.no. bs-0512R,1:100) (all from Beijing BIOSS Biotechnology Co., Ltd.).

2.6. Transcriptomic analysis

TRIzol ± reagent kit (Invitrogen; Thermo Fisher Scientific, Inc.) was used to extract total RNA from the rat renal cortex tissue. An Agilent 2100 BioAnalyzer (Agilent Technologies, Inc.) to assess the integrity of the RNA and subsequently isolated the Poly mRNA from total RNA using Oligo (dT) 25 beads. Enriched mRNA fragments were fragmented, and cDNA was synthesized by reverse transcription using random primers. The constructed libraries were sequenced using the Illumina HiSeq™ 2500 (Illumina, Inc.). The mRNA expression levels were ranked in descending order based on counts after normalization by FPKM.

Differentially expressed genes (DEGs) were defined as genes with a fold-change >1 and a FDR q-value <0.05, and DEGs were subsequently analyzed using Gene Ontology (GO) enrichment analysis.

A gene set related to ferroptosis was downloaded from the Ferroptosis Database V2 (http://www.zhounan.org/ferrdb/current/) as a background gene set. A sample expression matrix and a sample phenotype classification matrix were created. The Gene Set Enrichment Analysis software version 4.3.2 (GSEA, http://www.broadinstitute.org/gsea/index.jsp) [14] was employed to perform GSEA and determine the expression of genes related to ferroptosis in an academic context. Pathways with a p-value <0.05, a FDR q value < 0.25, and a |normalized enrichment score| >1 were considered significantly enriched.

An online plotting tool called Evenn (http://www.ehbio.com/test/venn#/) was utilized for the purpose of analyzing the association between the DEGs from each group and the ferroptosis-related genes.

2.7. Detection of serum and renal cortical homogenate lipid peroxide markers, and renal cortical iron ion concentration

Various biochemical assay kits were used to detect SOD(cat.no.A001-3), MDA(cat.no.A003-1), GSH(cat.no.A006-2-1)(all from Nanjing Jiancheng Biological Engineering Institute), total iron concentration (cat.no. PB1177W96), Fe2+ concentration (cat.no. PB1176W96) (all from Beijing perserbio Co.,Ltd) and GSH-Px(cat.no.TE0700, Leagene) levels.

2.8. Reverse transcription-quantitative PCR (RT-qPCR)

Based on the target genes, primer sequences were designed and synthesized for RT-qPCR. Total RNA was extracted from rat kidney tissues using TRIzol ± Universal total RNA extraction reagent (Tiangen Biotechnology Co., Ltd.). A RevertAid First Strand cDNA Synthesis Kit (cat. no. K1622; Thermo Fisher Scientific, Inc.) was used to synthesize cDNA. PCR was performed using a TB Green® Premix Ex Taq™ II (Tli RNaseH Plus) kit (Takara Bio, Inc.) on a Step One Plus Real-Time PCR instrument (Applied Biosystems). After detecting the Cq values for each template, the $2^{-\Delta\Delta Cq}$ method was used to calculate the relative expression [15]. The primer sequences are listed in Table 1.

2.9. Western blot analysis

The extraction of proteins from rat renal tissues was conducted using RIPA lysis and extraction buffer (Beijing Solarbio Technology Co., Ltd.). To measure the protein concentration of the samples, a BCA assay kit was used (Beyotime Institute of Biotechnology). After separation on a 10 % precast gel (cat.no.P01015, LABLEAD)in an electrophoresis apparatus (Bio-Rad Laboratories, Inc.), and

Table 1
The primers used for RT-qPCR analysis.

GENE	Forward Primer Sequence	Reverse Primer Sequence
SLC7A11	TACTGTCACTTTTTGGAGCCCTG	ATTACCAGCAGTTCCACCCAGAC
NCOA4	TGGCTCACCCCAAAACAGAC	AAAGAACTGGTGCTACAATGGCTAT
SLC3A2	GAAGGATGAAGTCAATGAAACCG	ATGCTCTTTTTCTTGGCACTTTG
GPX4	GAGGCAGGAGCCAGGAAGTAATC	CACGCAGCCGTTCTTATCAATG
SLC40A1	CCACTCTCTCTCCACTTGGGGGG	ACCAGAACAGAGCCTGCCACCAC
FTH1	TGCCAAATACTTTCTCCATCAATCTC	CCAGTCATCACGGTCAGGTTTC
TFR1	AATGGAAGACTCTGCTTTGCGACT	CTTACAATAGCCCAGGTAGCCGAT
SLC39A14	CTTTGGGGGTTTCTACCTTTTCTT	TGTCCGTGATGGTGCTCGTT
GAPDH	TTCAGCTCTGGGATGACCTT	TGCCACTCAGAAGACTGTGG

subsequently transferred to a PVDF membrane (Sinopharm Chemical Reagent Co., Ltd.), which was then blocked with 5 % skimmed milk in TBST (Sinopharm Chemical Reagent Co., Ltd.). Membranes were incubated with primary antibodies against System Xc- (cat.no. DF12509, Affinity Biosciences), GPX4 (cat.no. #59735, Cell Signaling Technology, Inc.), FTH1 (cat.no. #3998, Cell Signaling Technology, Inc.), SLC39A14 (cat.no. PA5-87880, Invitrogen; Thermo Fisher Scientific, Inc.), SLC40A1 (cat.no. ab239511, Abcam), TFR1 (cat.no. ab269513, Abcam) (all developed in rabbit; all used at a 1:1000 dilution), and GAPDH (cat.no. UM4002, Utibody) (developed in mouse, used at a 1:2000 dilution) were used to incubate the membranes overnight at 4 °C. Subsequently, the membranes were incubated with secondary antibodies bs-0295G-HRP and bs-0296G-HRP(both from Beijing BIOSS Biotechnology Co., Ltd.; both developed in goat; both used at a 1:3000 dilution) at room temperature for 2 h. Chemiluminescent detection was performed using an ECL kit (MilliporeSigma), and the films were scanned and archived in a fully automated chemiluminescence imaging system (Tanon Technology Co., Ltd.). Densitometry analysis was performed using ImageJ 1.51j8 (National Institutes of Health) and normalized to the respective GAPDH band.

2.10. Statistical analysis

All data were analyzed using GraphPad Prism version 8.0 (GraphPad Software, Inc.) and are presented as the mean ± standard deviation. Differences between two groups were compared using an independent samples *t*-test, while differences between multiple groups were compared using a one-way ANOVA followed by a post-hoc Tukey's test. $P < 0.05$ was considered to indicate a statistically significant difference.

3. Results

3.1. Changes in body weight, blood glucose, and 24-h urine protein levels in the DKD model

During modeling of DKD, significant changes were observed in the body weight, blood glucose levels, and 24-h urine protein concentration of the DKD group. The rats in the DKD group, after being provided with a high-fat diet for 18 weeks, exhibited a significantly higher body weight than those in the Control group ($P < 0.05$). However, after treatment with low-dose STZ solution was injected into the peritoneal cavity of DKD rats, with each weight measurement, a slow increase in body weight was observed in the Control group, but gradually decreased in the DKD group. The body weight of the DKD rats became lower than that of the Control group rats after the 21st week (shown in Fig. 3A). In addition, compared to the control group, the blood glucose levels of rats in the DKD group (consistently >16.7 mmol/L) were significantly higher ($P < 0.01$, shown in Fig. 3B). Furthermore, in the 23rd week, the DKD group rats exhibited a 24-h urine protein concentration of >30 mg, a significantly higher value than that observed in the Control group rats ($P < 0.01$, shown in Fig. 3C).

3.2. Changes in the physiological and hematological indices after intervention in each group

After 4 weeks of intervention, the DKD + Acu group exhibited a significant reduction in the left kidney weight, kidney index, blood urea nitrogen, serum creatinine, triglyceride levels (shown in Fig. 4A–E), 24-h urine protein, and blood glucose levels (shown in Fig. 4b and c) as compared with the DKD group ($P < 0.01$). This indicates that TLPW acupuncture has improved on glucose and lipid metabolism and reduced proteinuria in DKD rats. However, there were no significant differences in total cholesterol levels, total protein levels, albumin levels (shown in Fig. 4F–H), and weight (shown in Fig. 4A) between the DKD + Acu and DKD groups ($P > 0.05$).

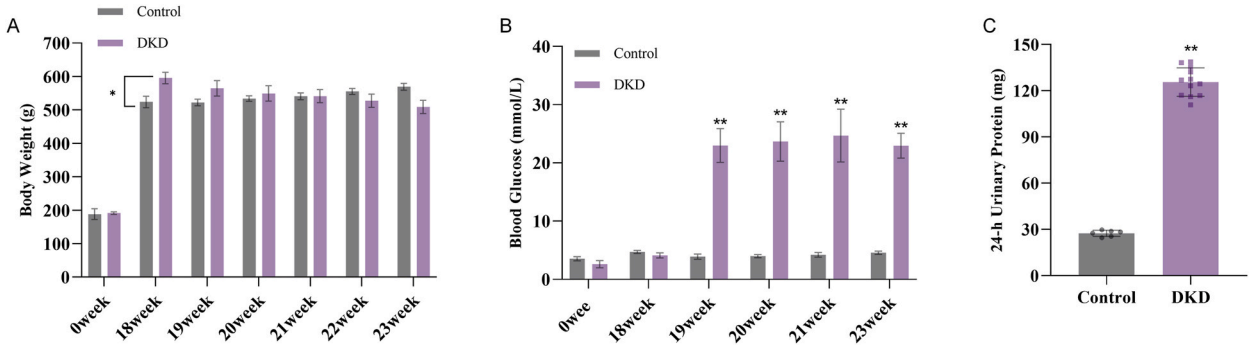

Fig. 3. Physiological indicators of DKD rats induced by high-fat diet and STZ.
Notes: (A) Body weight of the control group and DKD group from week 0–23; (B) Blood glucose levels of the control group and DKD group from week 0–23; (C) 24-h urinary protein quantification of the control group and DKD group at week 23.*$P < 0.05$ vs. Control group, **$P < 0.01$ vs. Control group; △$P < 0.05$ vs. DKD group, △△$P < 0.01$ vs. DKD group.

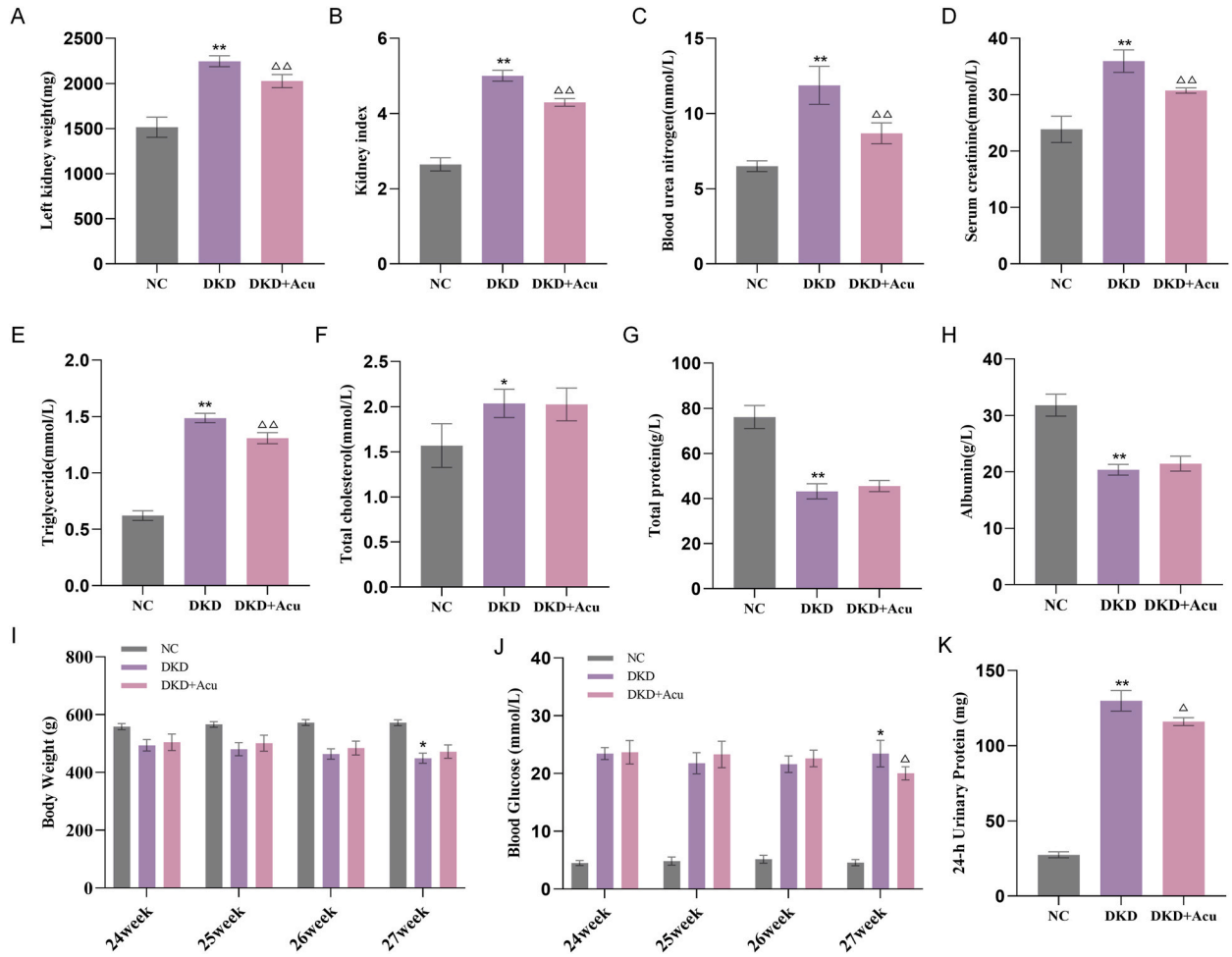

Fig. 4. Measurement of kidney parameters and biochemical indicators after 4 weeks intervention
Notes: (A) Left kidney weight (mg); (B) kidney index; (C) blood urea nitrogen (mmol/l); (D) serum creatinine (mmol/l); (E) triglycerides (mmol/l); (F) total cholesterol (mmol/l); (G) total protein (g/l); and (H) albumin (g/l) levels. (I) weight of the NC group, DKD group, and DKD + Acu group 4 weeks after acupuncture intervention; (J) blood glucose levels of the NC group, DKD group, and DKD + Acu group 4 weeks after acupuncture intervention. (K) 24-h urinary protein quantification of the NC group, DKD group, and DKD + Acu group 4 weeks after acupuncture intervention. $^{*}P < 0.05$ vs. Control group, $^{**}P < 0.01$ vs. Control group; $\triangle P < 0.05$ vs. DKD group, $\triangle\triangle P < 0.01$ vs. DKD group.

3.3. Pathological changes in each group after intervention

HE staining, PAS staining, and transmission electron microscopy were used to assess the rat kidney tissues. Pathological staining results showed that the DKD group exhibited pathological features such as thickening of the glomerular basement membrane, diffuse thickening of the capillary wall, and mesangial expansion compared to the NC group, while compared to the DKD group, the DKD + Acu group exhibited a decrease in the above pathological features (shown in Fig. 5A and B).Transmission electron microscopy (TEM) results showed that compared with the NC group, the DKD group exhibited thickening of the glomerular basement membrane, podocyte damage, fusion, destruction, or disappearance of foot processes. However, the DKD + Acu group showed a reduction in the fusion rate of foot processes, and an elevation in the number of foot processes when compared to the DKD group (shown in Fig. 5C).

3.4. Transcriptome analysis

RNA-seq was performed on rat kidney tissues and transcriptomic analysis was performed. A total of 3275 genes that were differentially expressed in the kidney tissues from the DKD group compared with the NC group were identified in the analysis. Of these genes, 1630 were upregulated, and 1645 were downregulated. In comparison, between the DKD group and the DKD + Acu group, there were 1012 DEGs, consisting of 473 upregulated DEGs and 539 downregulated DEGs (shown in Fig. 6A and B).

GO analysis of kidney tissues from the DKD group and DKD + Acu group showed significantly enriched pathways in the TLPW acupuncture-treated DKD group, which were closely related to adhesion of the cell in molecular function, that is to say, which were

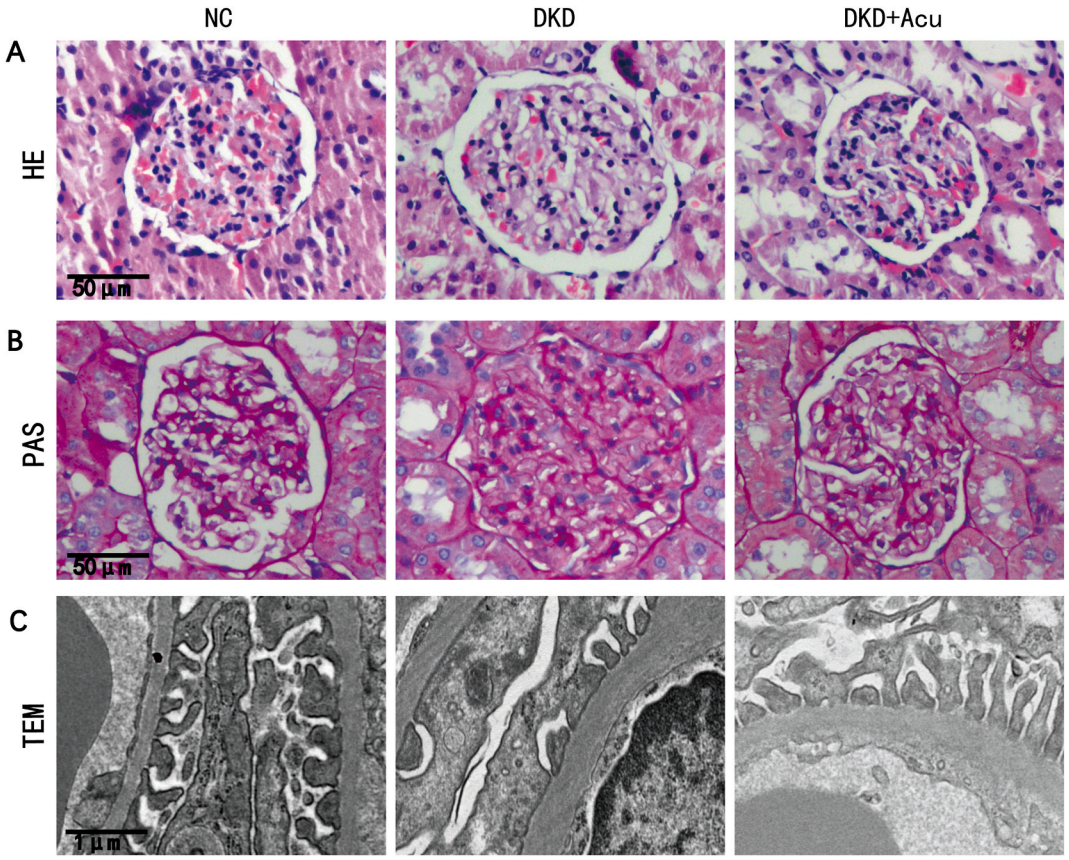

Fig. 5. Pathological changes in the glomerulus in the TLPW acupuncture intervention group after 4 weeks
Notes: (A) HE staining of the kidney tissues (scale bar, 50 μm). (B) PAS staining of the kidney tissues (scale bar, 50 μm). (C) TEM analysis of the kidney tissues (scale bar, 1 μm).

closely related to EMT, and then closely related to mitochondria in the cell composition, and closely associated with two critical steps of ferroptosis (iron ion transport and antioxidant system) as well as the binding of actin in the biological process (shown in Fig. 6C and D).

Through GSEA analysis, significant enrichment of genes in ferroptosis-related pathways in the NC vs. DKD group and DKD vs. DKD + Acu group was identified.

Intersection analysis using a Venn diagram of the DEGs related to ferroptosis in the kidney tissues of the three groups of rats revealed that there were 83 ferroptosis-related DEGs in the NC vs. DKD group, while in the DKD vs. DKD + Acu group, there were 26 ferroptosis-related DEGs (shown in Fig. 6G).

Therefore, it is hypothesized that TLPW acupuncture may reduce ferroptosis in the podocyte of DKD rats through the modulation of antioxidant stress and control of iron ion transport pathways, which in turn, reduced foot cell damage, proteinuria, and was closely associated with pathways such as EMT, mitochondrial respiratory chain, and actin breakdown.

3.5. Assessment of mitochondrial alterations and iron deposition

Transmission electron microscopy revealed mitochondrial alterations in the DKD group compared to the NC group, characterized by reduced mitochondrial volume, increased membrane density, and diminished cristae. However, these changes were mitigated in the DKD + Acu group. Additionally, Prussian blue staining indicated an increase in iron deposition in the renal tissues of the DKD group relative to the NC group. In contrast, the DKD + Acu group exhibited a reduction in iron deposition compared to the DKD group (shown in Fig. 7).

3.6. TLPW acupuncture alleviates ferroptosis

The results showed that in both kidney tissue and serum, the levels of GSH, GSH-px, and SOD were significantly reduced in the DKD group compared to the NC group ($P < 0.01$), while the MDA levels were higher than that in the NC group ($P < 0.01$). The levels of GSH, GSH-px, and SOD in the DKD + Acu group were higher than those in the DKD group ($P < 0.05$), while the MDA levels were lower than

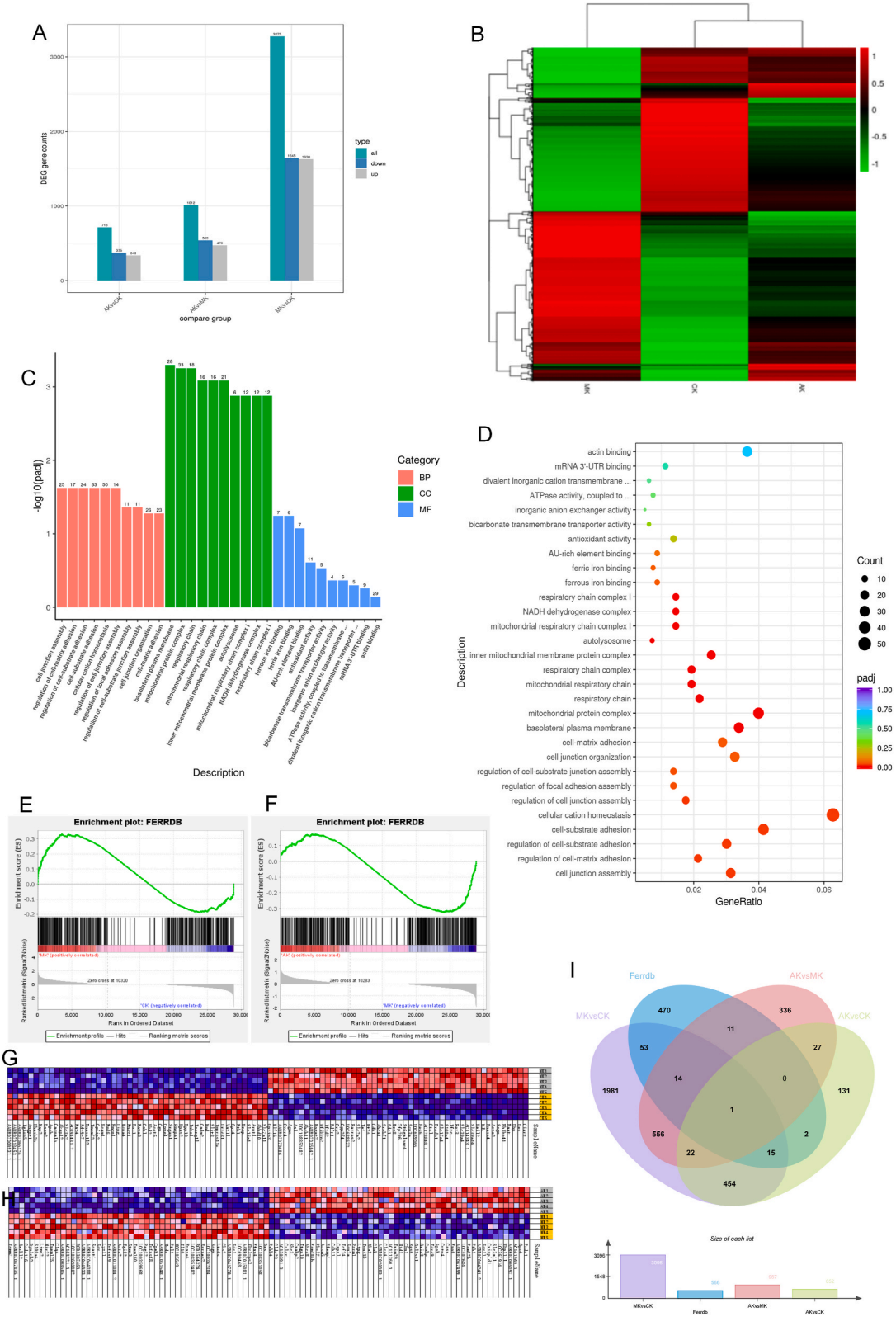

(caption on next page)

Fig. 6. Transcriptional analysis of differentially expressed genes, GO pathway analysis, and GSEA following TLPW acupuncture treatment
Notes: (A) Analysis of the number of differentially expressed genes between the NC group (n = 5), DKD group (n = 5), and DKD + Acu group (n = 5). (B) Heatmap of the differentially expressed genes between the NC group (n = 5), DKD group (n = 5), and DKD + Acu group (n = 5). (C) Bar plot of GO enrichment analysis between the DKD group and the DKD + Acu group. (D) Scatter plot of GO enrichment analysis between the DKD group and DKD + Acu group. (E) Line plot of GSEA between the NC group and DKD group. (F) Line plot of GSEA between the DKD group and DKD + Acu group. (G) Heatmap of GSEA between the NC group and DKD group. (H) Heatmap of GSEA between the DKD group and DKD + Acu group. (I) Venn diagram of genes with differential expression and genes related to ferroptosis in each group. CK: NC; MK: DKD; AK: DKD + Acu.

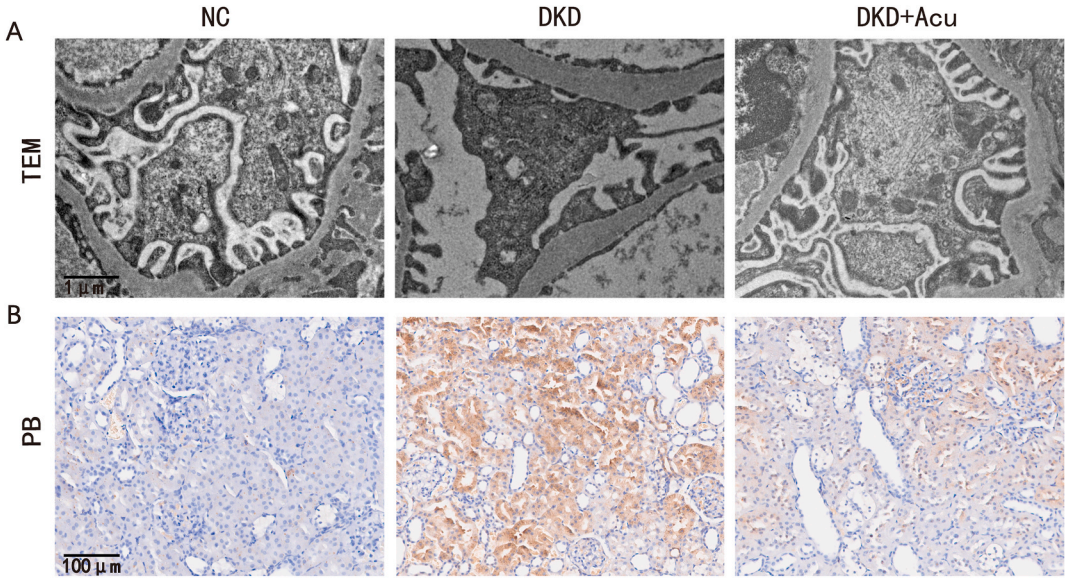

Fig. 7. Integrated electron microscopy and prussian blue staining of kidney tissues following 4 weeks of acupuncture treatment
Notes: (A) TEM analysis of the kidney tissues (scale bar, 1 μm). (B) Prussian blue staining of the kidney tissues (scale bar, 100 μm). (For interpretation of the references to colour in this figure legend, the reader is referred to the Web version of this article.)

that in the DKD group ($P < 0.05$) (shown in Fig. 8A–H). Both the total iron concentration and the Fe2+ concentration in the kidney tissues of the DKD group were found to be higher than that in the NC group. However, these concentrations in the DKD + Acu group were lower than in the DKD group ($P < 0.01$, as shown in Fig. 8I and J).

3.7. TLPW acupuncture suppresses oxidative stress pathways and regulates iron transport related pathways

The results of western blotting showed that the relative expression of both GPX4 and System Xc-were lower in the DKD group compared with the NC group ($P < 0.01$). Meanwhile, the results of PCR showed that the relative expression of GPX4, SLC3A2 and SLC7A11 were lower in the DKD group compared with the NC group ($P < 0.01$). However, in the DKD + Acu group, these levels were higher than those in the DKD group ($P < 0.05$) (shown in Fig. 9A–C,D).

The present study found that the DKD group exhibited higher relative expression levels of TfR1, SLC39A14 and NCOA4 in the kidney tissue compared with the NC group ($P < 0.01$). Conversely, the relative expression levels of FTH1 and SLC40A1 were lower than those in the NC group ($P < 0.01$). The results showed a noteworthy reduction in the relative expression levels of TfR1, SLC39A14 and NCOA4 in the DKD + Acu group compared with the DKD group ($P < 0.01$). Conversely, the relative expression levels of FTH1 and SLC40A1 were significantly higher than those in the DKD + Acu group than in the DKD group ($P < 0.05$) (shown in Fig. 9B–E,F).

3.8. Immunofluorescence analysis

According to the findings, the fluorescence intensity of TGF-β1 was observed to be higher in the DKD group than in the NC group ($P < 0.05$). However, a significant reduction in the fluorescence intensity was noted in the DKD + Acu group compared with the DKD group ($P < 0.05$). In the DKD group, the fluorescence intensity of Desmin ($P < 0.05$), α-SMA ($P < 0.05$), and Fsp1 ($P < 0.01$) was higher than the NC group. However, compared with the DKD group, the DKD + Acu group exhibited a reduction in the fluorescence intensity of Desmin ($P < 0.01$), α-SMA ($P < 0.05$), and Fsp1 ($P < 0.05$). These results suggest that TLPW acupuncture intervention can improve EMT in rats with diabetic nephropathy. In the DKD group, the fluorescence intensity of Nephrin ($P < 0.01$), Podocin ($P < 0.05$), and CD2AP ($P < 0.05$) was comparatively lower than that in the NC group, the fluorescence intensity of Nephrin ($P < 0.01$), Podocin ($P < 0.01$), and CD2AP ($P < 0.05$) in the DKD + Acu group was increased compared to the DKD group (shown in Fig. 10 and B).

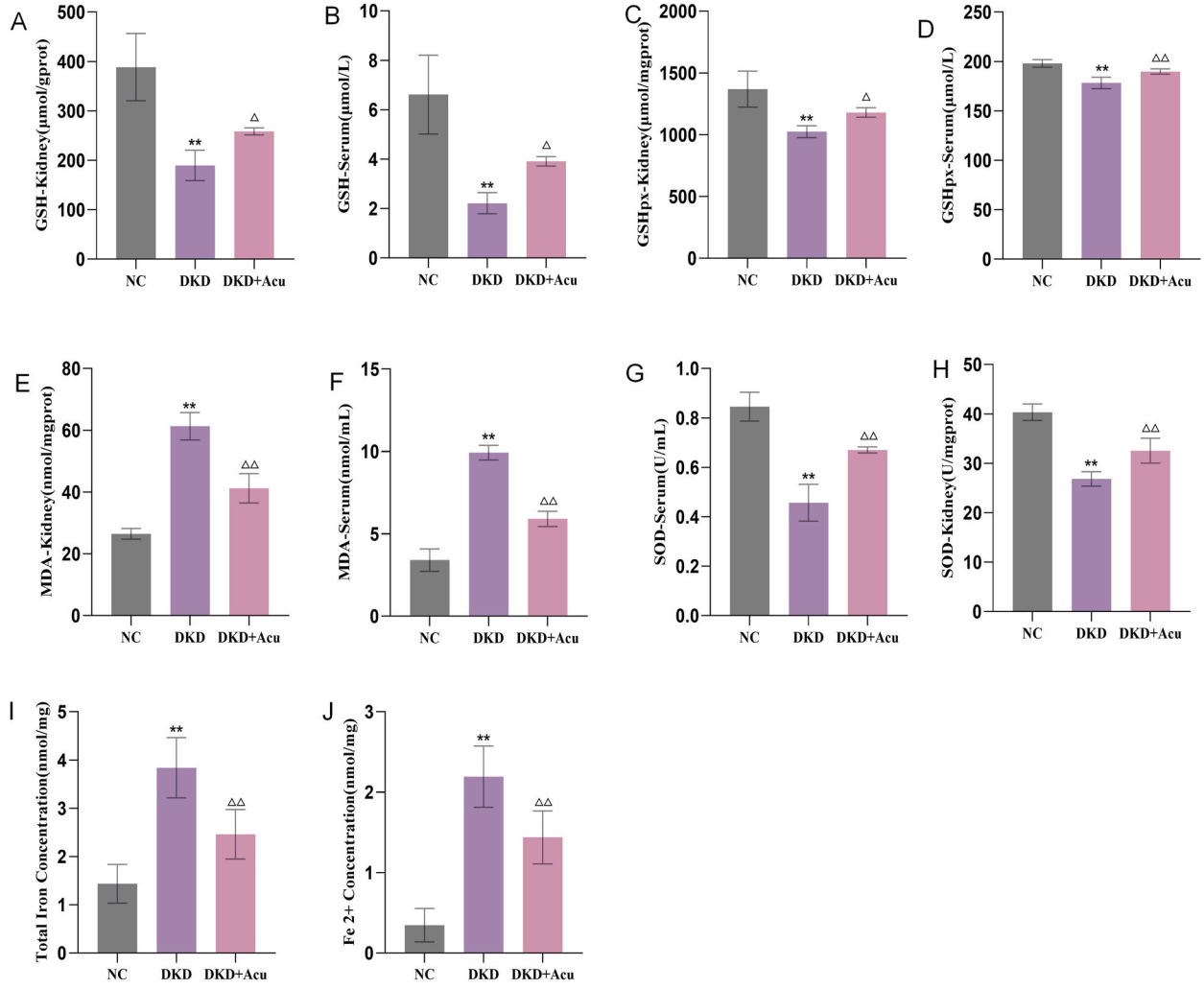

Fig. 8. Serum and renal oxidative stress-related indicators and iron ion concentrations
Notes: (A) Renal GSH levels. (B) Serum GSH levels. (C) Renal GSH-px levels. (D) Serum GSH-px levels. (E) Renal MDA levels. (F) Serum MDA levels. (G) Serum SOD levels. (H) Renal SOD levels. (I) Renal iron concentration. (J)Fe2+ concentration. $^{*}P < 0.05$ vs. Control group, $^{**}P < 0.01$ vs. Control group; $\triangle P < 0.05$ vs. DKD group, $\triangle\triangle P < 0.01$ vs. DKD group.

4. Discussion

Previous clinical and basic research has shown that acupuncture has a significant therapeutic effect on DKD [10–12], but its mechanism of action still remains incompletely understood and requires further investigation.

Recent discoveries have positioned ferroptosis at the heart of DKD pathology, with evidence from animal models pointing to its pivotal role in the disease's progression [16]. The underlying mechanisms involve disruptions in iron metabolism, increased lipid peroxidation, and depletion of antioxidant defenses, notably glutathione peroxidase 4 (GPX4) activity. These alterations not only underscore ferroptosis's contribution to the worsening of DKD but also open avenues for targeted therapeutic interventions aimed at mitigating ferroptosis [17].

Ferroptosis is a form of cell death that depends on lipid peroxidation and iron accumulation, and ferroptosis promotes the occurrence of DKD [5]. Through transcriptomic screening, critical targets of the TLPW acupuncture were identified in the oxidative stress pathways, iron transport pathways, and EMT pathways, then verified their molecular mechanisms.

Ferroptosis is intricately associated with oxidative stress. When oxidative stress occurs, a large amount of lipid peroxides are produced inside the cells, and the intracellular antioxidant system cannot remove lipid hydroperoxides (L-OOH) in a timely manner, leading to the accumulation of iron-dependent L-OOH to lethal levels, resulting in ferroptosis [18].

GPX4, with the assistance of reduced glutathione (GSH), alleviating lipid peroxidation and inhibiting ferroptosis [19,20]. System Xc-is composed of a heavy chain subunit 4F2hc (SLC3A2) and a light chain subunit xCT (SLC7A11), with SLC7A11 being the primary functional region responsible for cysteine/glutamate transport into the cell. Dicysteine taken up by the cell through System Xc-is

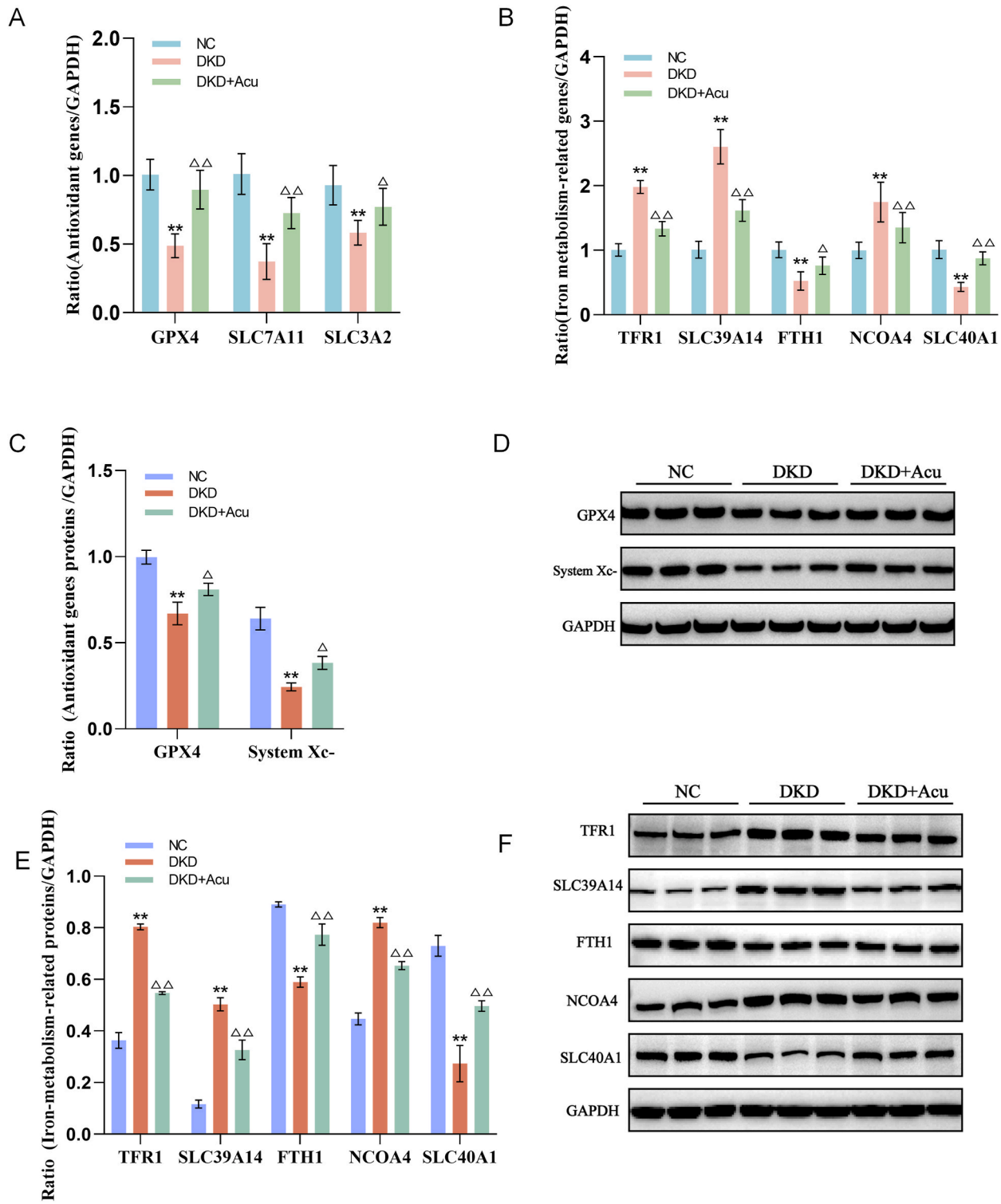

Fig. 9. Expression of antioxidant and iron ion transport-related genes and proteins

Notes: (A) PCR analysis of antioxidant genes and the ratio of antioxidant genes to GAPDH in the renal cortex. (B) Western blot of antioxidant genes and the ratio of antioxidant genes to GAPDH in the renal cortex. (C) PCR of iron metabolism-related genes and the ratio of iron metabolism-related genes to GAPDH in the renal cortex. (D) Western blot of iron metabolism-related genes and the ratio of iron metabolism-related genes to GAPDH in the renal cortex. *$P < 0.05$ vs. Control group, **$P < 0.01$ vs. Control group; △$P < 0.05$ vs. DKD group, △△$P < 0.01$ vs. DKD group.

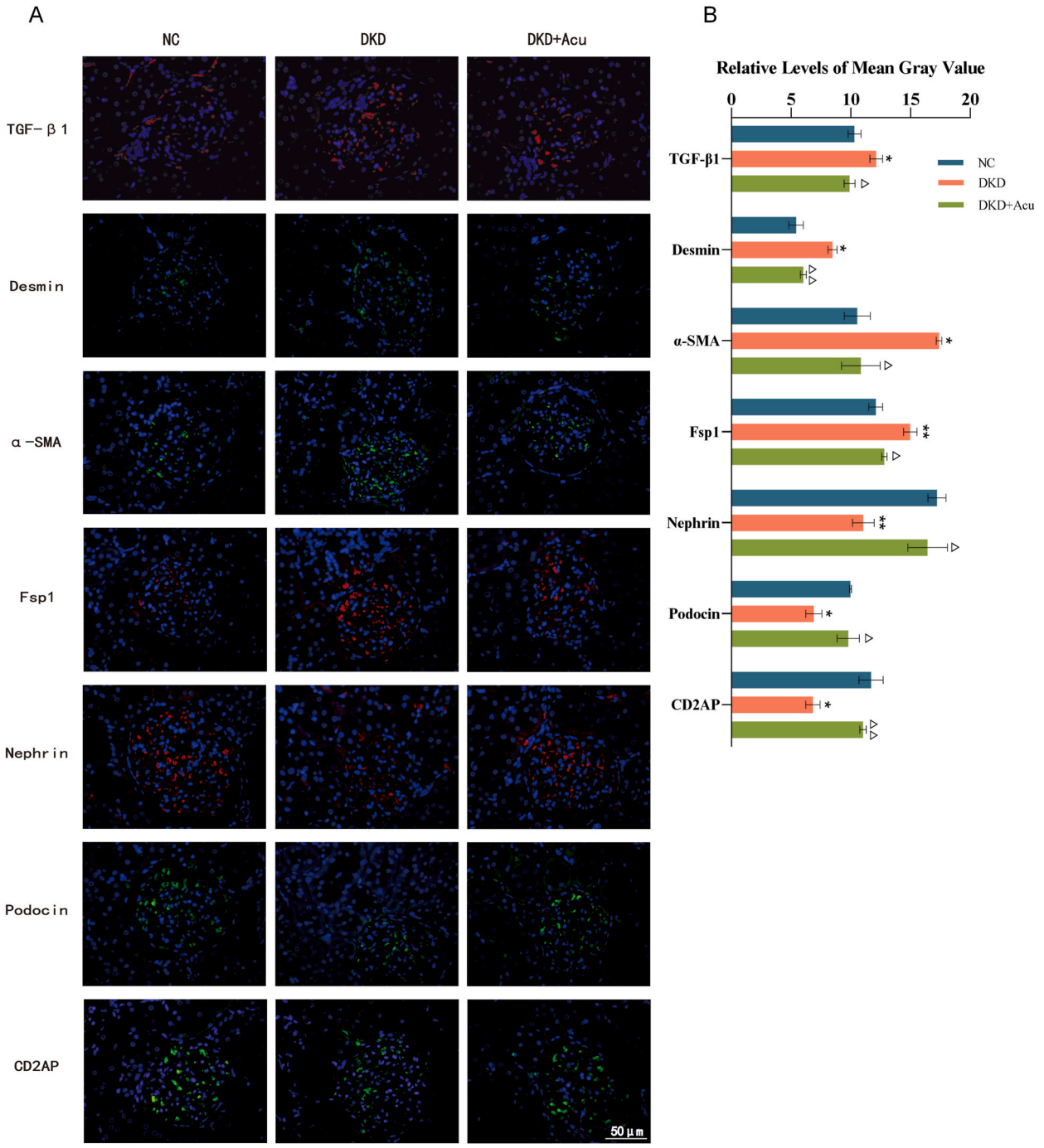

Fig. 10. TGF-β1, EMT (Desmin, α-SMA, and FSP1), and podocyte-specific markers (nephrin, podocin, and CD2AP) expression analysis in the renal cortex

Notes: (A) Expression of TGF-β1, EMT, and podocyte-specific markers through immunofluorescence analysis. (B) Relative mean gray value of TGF-β1, EMT, and podocyte-specific markers. *$P < 0.05$ vs. Control group, **$P < 0.01$ vs. Control group; △$P < 0.05$ vs. DKD group, △△$P < 0.01$ vs. DKD group.

reduced to cysteine in the cytoplasm through the consumption of NADPH [21]. System Xc-takes up cysteine from the extracellular environment in a 1:1 ratio and exports glutamate, thus controlling the rate of GSH biosynthesis and maintaining redox homeostasis [22]. Under conditions of oxidative stress, mammalian cells increase cysteine uptake through System Xc-to promote GSH synthesis [23], leading to increased GPX4 activity and enhanced cellular antioxidant capacity to inhibit ferroptosis.

Our results suggest that TLPW acupuncture can enhance the expression of GPX4 and System Xc-, thereby improving antioxidant

stress response and inhibiting ferroptosis.

On the other hand, the transport of iron ions provides the material basis for ferroptosis [24].

TfR1 mediates iron uptake in various cells, and the number of TfR1 molecules on the cell surface is the rate-limiting step for iron ion entry into cells, providing a condition for increased flux with excessive accumulation of Fe^{2+} in the cell [25,26]. Yasumura et al. [27] found that in both wild-type (WT) and heterozygous transferrin receptor 1-deficient (TfR1+/−) mice with unilateral ureteral obstruction-induced renal fibrosis and deoxycorticosterone acetate (DOCA)-salt-induced DKD, TfR1 ± mice had inhibited renal fibrosis compared with WT mice.

SLC39A14 is a divalent iron importer located in the proximal and distal tubules and is involved in NTBI uptake in the lumen. The protein SLC39A14 plays a critical role in facilitating the transportation of divalent iron in the proximal and distal tubules of the kidneys, as well as aiding in the uptake of NTBI in the lumen. Wu et al. [28] found that SLC39A14 expression was increased in humans with DKD and in DKD rat models, both *in vivo* and *in vitro*.

As ferritin heavy chain, Fth1 was degraded in the autophagic lysosome, and Fe^{2+} is rapidly released after the degradation, leading to cellular iron overload and thus promoting iron-induced cell death [29,30]. Ferroportin (SLC40A1/FPN) is the only known iron export membrane protein in mammals. When iron overload occurs, Fe^{2+} is primarily exported by SLC40A1 in the cell membrane [31].

The results of the present study showed that the TLPW acupuncture technique inhibited iron-induced cell death by restoring iron homeostasis to a certain extent by decreasing the expression of TfR1 and SLC39A14 and increasing the expression of FTH1 and SLC40A1.

According to a previous study, intercellular contacts of epithelial cells inhibit ferroptosis [32]. In contrast, cells in a mesenchymal state are more prone to ferroptosis due to the loss of intercellular communications and the activation of EMT factors [33]. In the process of DKD, activated fibroblasts transform into myofibroblasts and secrete ECM, promoting renal fibrosis [34]. EMT widely participates in this process [35], which also becomes an essential factor leading to the thickening of the GBM and aggravating podocyte injury [36].

Hyperglycemia can participate in the progression of DKD through TGF-β1 [33]. TGF-β1 promotes cell transformation into myofibroblasts through pathways such as activating the Smad complex, inducing the expression of fibrosis transcription factors and integrates with the regulatory elements in the gene promoter region to regulate the expression of EMT-related complex after entering the nucleus, aggravating renal fibrosis,EMT and DKD progression [37–39].

EMT of podocytes leads to foot process fusion, loss of slit diaphragm, reduction of slit diaphragm structural proteins such as Nephrin, Podocin, and CD2AP, downregulation of foot cell phenotype markers, and rearrangement of the cytoskeleton of myofibrils. The expression of mesenchymal cell markers such as desmin, FSP-1, and α-SMA is up-regulated [40]. Damaged foot cells detach from the GBM, the number of foot cells decreases, the GBM is exposed, and the glomerular filtration membrane is impaired, resulting in proteinuria and ultimately leading to DKD.

The results of the present study show that the TLPW acupuncture technique can also alleviate EMT and inhibit DKD by inhibiting the expression of TGF-β1, desmin, FSP-1, and α-SMA, increasing the expression of Nephrin, Podocin, and CD2AP, and restoring the structure of foot processes in cells.

In summary, this study demonstrated that TLPW acupuncture enhanced the antioxidant stress response of podocytes, restored iron homeostasis, inhibited EMT, and suppressed iron-induced cell death, leading to improvements in podocyte structure, restoration of filtration function, reduction of proteinuria, and prevention of the progression of DKD.

5. Conclusion

TLPW acupuncture improves proteinuria in diabetic kidney disease rats by inhibiting ferroptosis through GPX4/System Xc- and TfR1/SLC39A14/FTH1/SLC40A1 signal pathways.

Statement

The study protocol used in the present study was approved by the Ethics Committee of the Institute of Radiation Medicine, Chinese Academy of Medical Sciences (approval no. IRM-DWLL-2019103).

Funding sources

This work was supported by the National Natural Science Foundation of China [grant number 81904296].

Data availability statement

The datasets used and/or analyzed during the current study are available from the corresponding author upon reasonable request.

CRediT authorship contribution statement

J.I. Yue: Writing – original draft, Investigation, Funding acquisition, Data curation, Conceptualization. **Z.H.A.N.G. Xin-yuan:** Validation, Investigation, Data curation. **X.I.A.O. Yun-ming:** Investigation, Formal analysis, Data curation. **Z.H.U.A.N.G. Zi-hao:** Investigation, Formal analysis, Data curation. **Y.A.N.G. Xiao-hui:** Investigation, Formal analysis, Data curation. **L.I. Xin-ju:** Writing –

review & editing, Supervision, Funding acquisition, Data curation, Conceptualization.

Declaration of competing interest

The authors declare that they have no known competing financial interests or personal relationships that could have appeared to influence the work reported in this paper.

Appendix A. Supplementary data

Supplementary data to this article can be found online at https://doi.org/10.1016/j.heliyon.2024.e33675.

References

[1] K. Umanath, J.B. Lewis, Update on diabetic nephropathy: core curriculum 2018, Am. J. Kidney Dis. 71 (2018) 884–895.
[2] H. Sun, P. Saeedi, S. Karuranga, M. Pinkepank, K. Ogurtsova, B.B. Duncan, et al., IDF Diabetes Atlas: global, regional and country-level diabetes prevalence estimates for 2021 and projections for 2045, Diabetes Res. Clin. Pract. 183 (2022) 109–119.
[3] A.M. Mottl, R. Alicic, C. Argyropoulos, F.C. Brosius, M. Mauer, M. Molitch, et al., KDOQI US commentary on the KDIGO 2020 clinical practice guideline for diabetes management in CKD, Am. J. Kidney Dis. 79 (2022) 457–479.
[4] A.A. Ahmad, S.O. Draves, M. Rosca, Mitochondria in diabetic kidney disease, Cells 10 (2021) 2945.
[5] Y. Wu, Y. Chen, Research progress on ferroptosis in diabetic kidney disease, Front. Endocrinol. 13 (2022).
[6] X. Chen, C.H. Yu, R. Kang, D.L. Tang, Iron metabolism in ferroptosis, Front. Cell Dev. Biol. 8 (2020).
[7] B.R. Stockwell, Ferroptosis turns 10: emerging mechanisms, physiological functions, and therapeutic applications, Cell 185 (2022) 2401–2421.
[8] X.J. Liu, X.K. Hu, H. Yang, L.M. Gui, Z.X. Cai, M.S. Qi, et al., A review of traditional Chinese medicine on treatment of diabetic nephropathy and the involved mechanisms, Am. J. Chin. Med. 50 (2022) 1739–1779.
[9] W. Xiong, F.F. He, R.Y. You, J. Xiong, Y.M. Wang, C. Zhang, et al., Acupuncture application in chronic kidney disease and its potential mechanisms, Am. J. Chin. Med. 46 (2018) 1169–1185.
[10] Z.L. Zhang, X.Q. Ji, P. Zhang, X.H. Zhang, Z.J. Meng, X.J. Yang, Randomized and controlled study on needling method of harmonizing spleen-stomach for early intervention of diabetic nephropathies and the mechanism of protecting kidney, Zhongguo zhen jiu = Chinese acupuncture & moxibustion 27 (2007) 875–880.
[11] M. Wang, Z.L. Zhang, X.Q. Ji, Y.Q. Yang, X.J. Yang, S. Li, Randomized controlled clinical trial for analyzing effect of "spleen- stomach regulation needling" on oxidative stress level in patients with diabetic nephropathy, Acupunct. Res. 40 (2015) 409–441.
[12] Z.L. Zhang, X.J. Li, L. Liu, J.Y. Sun, X. Wang, Z.H. Zhao, et al., Tiaolipiwei acupuncture reduces albuminuria by alleviating podocyte lesions in a rat model of diabetic nephropathy, Evid. base Compl. Alternative Med. 2018 (2018) 1913691.
[13] X.X. Guo, Y. Wang, K. Wang, B.P. Ji, F. Zhou, Stability of a type 2 diabetes rat model induced by high-fat diet feeding with low-dose streptozotocin injection, J. Zhejiang Univ. - Sci. B 7 (2018) 559–569.
[14] S. Aravind, T. Pablo, K.M. Vamsi, M. Sayan, L.E. Benjamin, A.G. Michael, et al., Gene Set Enrichment Analysis: A Knowledge-Based Approach for Interpreting Genome-wide Expression Profiles, vol. 102, Proceedings of the National Academy of Sciences, 2005, pp. 15545–15550.
[15] K.J. Livak, T.D. Schmittgen, Analysis of relative gene expression data using real-time quantitative PCR and the $2^{-\Delta\Delta CT}$ method, Methods 25 (2001) 402–408.
[16] J.L. Li, L.X. Li, Z. Zhang, P.J. Chen, H.Y. Shu, C. Yang, et al., Ferroptosis: an important player in the inflammatory response in diabetic nephropathy, Front. Immunol. 14 (2023).
[17] Y. Wu, Y. Chen, Research progress on ferroptosis in diabetic kidney disease, Front. Endocrinol. 13 (2022).
[18] H. Flores-Romero, U. Ros, A.J. García-Sáez, Chapter Six-A lipid perspective on regulated cell death, International Review of Cell and Molecular Biology 351 (2020) 197–236.
[19] B.R. Stockwell, J.P.F. Angeli, H. Bayir, A.I. Bush, M. Conrad, S.C. Dixon, et al., Ferroptosis: a regulated cell death nexus linking metabolism, redox biology, and disease, Cell 171 (2017) 273–285.
[20] X.G. Liu, Y.L. Zhang, L. Zhuang, K. Olszewski, B.Y. Gan, NADPH debt drives redox bankruptcy: SLC7A11/xCT-mediated cystine uptake as a double-edged sword in cellular redox regulation, Genes & Diseases 8 (2021) 731–745.
[21] P. Koppula, L. Zhuang, B.Y. Gan, Cystine transporter SLC7A11/xCT in cancer: ferroptosis, nutrient dependency, and cancer therapy, Protein & Cell 12 (2021) 599–620.
[22] R.J. Bridges, N.R. Natale, S.A. Patel, System xc^- cystine/glutamate antiporter: an update on molecular pharmacology and roles within the CNS, Br. J. Pharmacol. 165 (2012) 20–34.
[23] J.L. Parker, J.C. Deme, D. Kolokouris, G. Kuteyi, P.C. Biggin, S.M. Lea, et al., Molecular basis for redox control by the human cystine/glutamate antiporter system xc, Nat. Commun. 12 (2021) 7147.
[24] M. Morales, X. Xue, Targeting iron metabolism in cancer therapy, Theranostics 11 (2021) 8412–8429.
[25] P.V. Candelaria, L.S. Leoh, M.L. Penichet, T.R. Daniels-Wells, Antibodies targeting the transferrin receptor 1 (TfR1) as direct anti-cancer agents, Front. Immunol. 12 (2021).
[26] Nan Huang, L.L. Zhan, Y. Cheng, X.L. Wang, Y.X. Wei, Q. Wang, et al., TfR1 extensively regulates the expression of genes associated with ion transport and immunity, Current Medical Science 40 (2020) 493–501.
[27] S. Yasumura, Y. Naito, K. Okuno, H. Sawada, M. Asakura, T. Masuyama, Effects of heterozygous TfR1 (transferrin receptor 1) deletion in pathogenesis of renal fibrosis in mice, Hypertension 75 (2020) 413–421.
[28] K. Wu, L.Y. Fei, X.H. Wang, Y. Lei, L. Yu, W.Q. Xu, et al., ZIP14 is involved in iron deposition and triggers ferroptosis in diabetic nephropathy, Metallomics 14 (2022) mfac034.
[29] Y.Y. Fang, X.C. Chen, Q.Y. Tan, H.H. Zhou, J. Xu, Q. Gu, Inhibiting ferroptosis through disrupting the NCOA4–FTH1 interaction: a new mechanism of action, ACS Cent. Sci. 7 (2021) 980–989.
[30] J.D. Mancias, X.X. Wang, S.P. Gygi, J.W. Harper, A.C. Kimmelman, Quantitative proteomics identifies NCOA4 as the cargo receptor mediating ferritinophagy, Nature 509 (2014) 105–109.
[31] L. Jiang, J.M. Wang, K. Wang, H. Wang, Q. Wu, C. Yang, et al., RNF217 regulates iron homeostasis through its E3 ubiquitin ligase activity by modulating ferroportin degradation, Blood 138 (2021) 689–705.
[32] J. Wu, A.M. Minikes, M.H. Gao, H.J. Bian, Y. Li, B.R. Stockwell, et al., Intercellular interaction dictates cancer cell ferroptosis via NF2–YAP signalling, Nature 572 (2019) 402–406.
[33] Xin Chen, R. Kang, G. Kroemer, D.L. Tang, Broadening horizons: the role of ferroptosis in cancer, Nat. Rev. Clin. Oncol. 18 (2021) 280–296.
[34] T. Kisseleva, D.A. Brenner, Is it the end of the line for the EMT? Hepatology 53 (2011) 1433–1435.
[35] C. Kuppe, M.M. Ibrahim, J. Kranz, X.T. Zhang, S. Ziegler, J. Perales-Patón, et al., Decoding myofibroblast origins in human kidney fibrosis, Nature 589 (2021) 281–286.

[36] M.Q. Tian, L. Zhang, M. Zhang, L.W. Qiao, B.Q. Xu, C. Li, et al., JLP/Foxk1/N-cadherin axis fosters a partial epithelial-mesenchymal transition state in epithelial tubular cells, iScience 26 (2023) 106396.
[37] K.K. Kim, D. Sheppard, H.A. Chapman, TGF-β1 signaling and tissue fibrosis, Cold Spring Harb Perspect Biol 10 (2018).
[38] C.H. Ong, C.L. Tham, H.H. Harith, N. Firdaus, D.A. Israf, TGF-β-induced fibrosis: a review on the underlying mechanism and potential therapeutic strategies, Eur. J. Pharmacol. 911 (2021) 174510.
[39] Q.D. Ying, G.Z. Wu, Molecular mechanisms involved in podocyte EMT and concomitant diabetic kidney diseases: an update, Ren. Fail. 39 (2017) 474–483.
[40] C.J. May, M. Saleem, G.I. Welsh, Podocyte dedifferentiation: a specialized process for a specialized cell, Front. Endocrinol. 5 (2014).